An investigation of density fluctuations and electron transport in the Madison Symmetric Torus reversed-field pinch

N. E. Lanier[a)]
Los Alamos National Laboratory, Los Alamos, New Mexico 87545

D. Craig, J. K. Anderson, T. M. Biewer, B. E. Chapman, D. J. Den Hartog, C. B. Forest, and S. C. Prager
Department of Physics, University of Wisconsin–Madison, Madison, Wisconsin 53706

D. L. Brower and Y. Jiang
Department of Electrical Engineering, University of California at Los Angeles, Los Angeles, California 90095-1594

(Received 27 December 2000; accepted 18 April 2001)

The origin of large scale density fluctuations and their role in electron transport has been investigated in the Madison Symmetric Torus reversed-field pinch [R. N. Dexter *et al.*, Fusion Tech. **19**, 131 (1991)]. At medium frequencies (10–30 kHz), $\tilde{n}$ is associated with core-resonant magnetic fluctuations having poloidal mode number $m=1$ and toroidal mode numbers $n=6-10$. These chord-averaged density fluctuations are shown to be coherent with large scale radial flow fluctuations, permitting fluctuation-induced particle flux of the form $\langle \tilde{n}\tilde{v}_r \rangle$ to be studied. In the edge, although amplitudes are large, $\tilde{n}$ and $\tilde{v}_r$ are out of phase, consistent with advection of the mean density gradient by perturbed magnetic field lines and no electron transport. During improved confinement discharges, produced by inductive current drive, both fluctuation amplitudes and the total radial electron flux are greatly reduced over the entire plasma cross section. © *2001 American Institute of Physics.* [DOI: 10.1063/1.1378328]

I. INTRODUCTION

The strategy for managing fluctuation-induced electron transport in magnetically confined plasmas consists of three parts: characterizing the origin of density fluctuations, understanding the link between these fluctuations and electron transport, and developing methods for controlling the fluctuations that cause transport. These issues are of particular importance for the reversed-field pinch (RFP)[1] in which magnetic and electrostatic fluctuations are believed to drive substantial particle and energy transport. Although there is much circumstantial evidence for fluctuation-induced electron transport throughout the plasma, direct measurements have been limited to the plasma edge. These studies concluded that the particle[2] and heat[3] transport due to magnetic fluctuations are both small in the edge of the RFP but that electrostatic fluctuation-induced particle transport is large.[4,5] The best indication that fluctuations contribute to transport in the core comes from the observation that modifying the current density profile to reduce core-resonant magnetic fluctuations also reduces anomalous energy and particle transport.[6–8]

In this paper, we examine large-scale density fluctuations throughout the plasma using a high speed multichord far-infrared (FIR) laser interferometer. Interferometry has been used previously to study density fluctuations[9–11] and their relationship to transport[12–14] for standard discharges in the ZT-40M RFP.[15] In the present study, we investigate the spectral content and underlying cause of the measured density fluctuations, the link between these fluctuations and electron transport, and the reduction of both fluctuations and electron transport via current profile modification.

To understand the origin of the measured density fluctuations, we make extensive use of correlation techniques. Correlations between toroidally and poloidally displaced interferometer chords yield toroidal and poloidal wave number spectra. The links between magnetic and density fluctuations are investigated by correlating individual FIR chords with an array of magnetic coils. Finally, we gain insight into the origin of density fluctuations by correlating the interferometer chords with chordal measurements of the radial flow velocity. Moreover, this correlated product of density and radial velocity fluctuations also yields an important component of the fluctuation-induced particle flux.

Using these techniques in the Madison Symmetric Torus (MST),[16] we find that large-scale density fluctuations ($\tilde{n}$) fall naturally into three groups corresponding to low, medium, and high frequencies. Low frequency fluctuations (<10 kHz) result from both time variation of the spatial mean and poloidally symmetric fluctuations resonant in the edge. Density fluctuations at medium frequencies (10–30 kHz), are coherent with the core-resonant magnetic tearing modes and have poloidal mode number $m=1$ and toroidal mode numbers $n=6-10$. Though resonant in the core, these fluctuations are truly global, extending out to the edge, and play a central role in RFP confinement. At frequencies above 30 kHz, $\tilde{n}$ is composed primarily of edge $m=1$ fluctuations

a)Electronic mail: nlanier@lanl.gov

with a broad toroidal mode number spectrum.

In the medium frequency range, density and magnetic fluctuations are very coherent. By correlating individual interferometer chords with individual toroidal harmonics, obtained from a magnetic coil array, we can extract the density fluctuation associated with each core-resonant mode. Upon inversion we obtain radial profiles of the density fluctuation amplitude. We observe that the density fluctuation profiles are generally hollow and are more hollow for larger toroidal mode numbers. The hollow profiles are the result of a large advective component—the large equilibrium density gradient in the edge being deformed in space by the perturbed magnetic field lines. The fact that the profiles are more hollow for higher n numbers is consistent with the expectation from magnetohydrodynamic (MHD) computation that the peak of the radial magnetic fluctuation profiles move out in radius for higher n.

Chord-integrated density and radial velocity fluctuation measurements are also coherent in the medium frequency range, thus permitting fluctuation-induced transport ($\langle \tilde{n}\tilde{v}_r \rangle$) resulting from core-resonant modes to be studied. In the edge, $\tilde{n}$ and $\tilde{v}_r$ have large amplitudes but are $\pi/2$ rad out of phase, which is consistent with both advection of the mean density gradient by perturbed magnetic field lines and no particle transport. This, in combination with earlier probe measurements, demonstrates that core-resonant modes do not produce any measurable edge transport of any kind—magnetic or electrostatic. In the core, the velocity measurements are difficult to interpret conclusively (due to the effects of chord averaging) but suggest that density and flow fluctuations are in phase, implying fluctuation-induced electron transport by core-resonant modes. Estimates of core fluctuation amplitudes indicate that the total electron flux measured in the core could be accounted for by fluctuations of this type. These measurements support the notion that transport is accomplished by locally resonant modes.

Using pulsed poloidal current drive (PPCD) in MST, discharges with reduced magnetic fluctuations and improved confinement can be obtained.[6,7] We observe that the equilibrium radial electron flux is reduced more than an order of magnitude in these discharges. Concurrent with this change, density fluctuations in all frequency ranges and at all radii are reduced. Moreover in the medium frequency range, the phase of the core-resonant density fluctuations change by $\pi/2$ rad relative to the edge. This indicates a change in the origin of the fluctuations and, when combined with the amplitude reduction, a reduction of core fluctuation-induced electron transport by core-resonant modes. This constitutes the first direct measurement of reduced core fluctuations and electron transport in PPCD discharges.

In what follows, we describe the diagnostics (Sec. II) and analysis techniques (Sec. III) employed in this work. We then present in Sec. IV, the wave number and frequency decomposition of the measured density fluctuations. The relationship between density and magnetic fluctuations, including radial profiles of individual core-resonant density fluctuations, is presented in Sec. V. The connection between density and velocity fluctuations and the resulting fluctuation-induced electron flux is presented in Sec. VI. Finally in Sec. VII, we report on the reduction of density fluctuations and total electron fluxes in discharges with reduced magnetic fluctuations and transport during auxiliary current drive experiments.

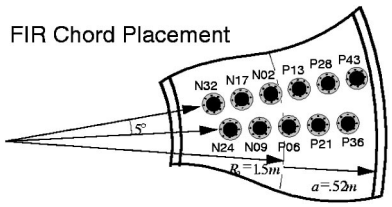

FIG. 1. The 11 FIR chords are segmented into two arrays separated toroidally by 5°.

II. DIAGNOSTICS

Determination of the density fluctuation origin and the resulting fluctuation-induced transport requires simultaneous measurements of density, radial velocity, and magnetic field fluctuations, as well as the electron ionization source profile. For a complete description of the diagnostics and analysis techniques the reader is referred to Ref. 17. Here we briefly describe the interferometer used to measure density fluctuations, the Doppler spectrometer for impurity ion flow velocity fluctuations, and the magnetic coil array for magnetic fluctuations. We also describe the H_α and soft x-ray arrays which provide a measure of the electron source profile based on electron ionization from neutral hydrogen or deuterium and impurities.

A. The far-infrared interferometer

The FIR laser interferometer is a vertically viewing heterodyne system[18,19] that measures chord-averaged electron density ($\bar{n}$),

$$\bar{n} = \left[\int_{-L/2}^{+L/2} n_e(z)\,dz \right] \Big/ L, \tag{1}$$

where z is the vertical coordinate, and L is the chord length through the plasma. The dual laser cavities are operated at wavelengths near $\sim$432.5 μm (694 GHz) with a 750 kHz interference frequency. Eleven chords are separated into two arrays (Fig. 1), toroidally displaced by 5°, viewing impact parameters ranging from $r/a=0.62$ inboard to $r/a=0.83$ outboard, where a is the plasma minor radius ($a=0.52$ m). With the assumption of up–down symmetry, these chord-integrated measurements can be inverted to yield equilibrium electron density profiles.

A digital phase extraction technique[20,21] is used to provide a high frequency response for the study of density fluctuations. With a maximum frequency response exceeding 500 kHz, the primary limitation of the system becomes the chord-averaged nature of the measurement, which severely attenuates the small-scale fluctuations with frequencies greater than 200 kHz. This attenuation is observed when comparing the power spectra from the FIR and edge Langmuir probe measurements. Because of the insensitivity to

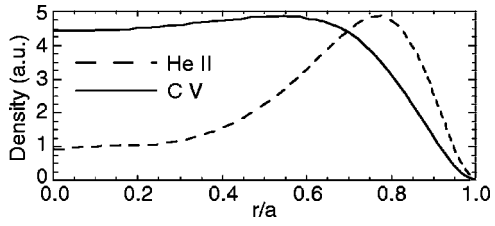

FIG. 2. Impurity profiles of C V and He II for standard confinement low current plasma discharges, computed from MIST.

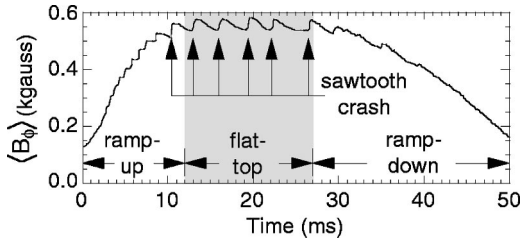

FIG. 3. Average toroidal magnetic field vs time, illustrating the regularity of sawteeth during the flattop phase of the discharge. Sawteeth provide excellent benchmarks for ensemble averaging.

very high frequency, the FIR system is typically operated with a frequency response of 250 kHz, which is well suited for the detection of the large-scale, lower frequency (<30 kHz) fluctuations that are dominant in the MST.

B. The Ion Dynamics Spectrometer (IDS)

The Ion Dynamics Spectrometer[22,23] is a custom designed, high throughput, Doppler spectrometer that measures chord-averaged impurity ion temperature and flow. The fast time resolution (~ 10 μs) allows the IDS to resolve radial velocity fluctuations relevant to fluctuation-induced transport. Though a chord-averaging diagnostic, radial localization can be enhanced by monitoring different impurities and charge states. For example, He II, which is primarily located at $r/a>0.6$ (Fig. 2), provides an excellent measurement of $\tilde{v}_r$ in the edge. Measurements of $\tilde{v}_r$ in the core are made by monitoring C V, which has a broad, flat profile inside r/a of 0.8.

C. Magnetic coil arrays

The dominant magnetic fluctuations in MST arise from the core-resonant resistive tearing modes. These modes are global and are monitored by an extensive array of magnetic pickup coils located at the plasma boundary. A 32-position toroidal array and a 16-position poloidal array are available to monitor the equilibrium and fluctuating magnetic fields. The multicoil array permits the magnetic fluctuations to be decomposed into their Fourier harmonics, allowing the poloidal (m) and toroidal (n) mode number spectra to be determined.

D. Multichord $H_\alpha(D_\alpha)$ array

The electron source profile from neutral hydrogen or deuterium is measured with a nine-chord array of filtered monochromators that detect $H_\alpha(D_\alpha)$ emission. The monochromators, designed for simplicity, utilize a narrow bandpass filter and a high speed photodiode to make quantitative measurements of $H_\alpha(D_\alpha)$ photons. For the temperatures of MST plasmas, the (H_α) emission is proportional to the ionization of neutral hydrogen.[24] Signals from the multichord system are inverted to yield local source rates from neutral hydrogen. A novel feature of the $H_\alpha(D_\alpha)$ array is its collinear arrangement with the FIR interferometer (meaning the H_α detector looks along the same chord as the FIR interferometer). By simultaneously measuring electron density and hydrogen ionization in each chord, asymmetric sourcing issues become much less important when calculating the radial electron flux.

E. X-ray diagnostics

Plasma electrons are also generated by ionization of impurities. In MST, the dominant contributions arise from aluminum, carbon, and oxygen. Three soft x-ray filtered spectrometers,[25] collecting light from three chords viewing impact parameters of $r/a=0.02$, 0.40, and 0.77, are used for absolute flux measurements from K shell transitions of Al XII, O VII, O VIII, C V, and C VI. Transitions from these states are well characterized, and the absolute flux measurements can be converted into impurity charge state densities. This information, along with electron density and temperature measurements, is used to constrain impurity fractions via the Multi-Ion Species Transport (MIST) code.[26] In general, electron sourcing from impurities in standard-confinement discharges is negligible when compared to the contribution from ionization of neutral hydrogen. However, during PPCD, neutral hydrogen densities in the core drop to such low levels that sourcing from impurities becomes important.

III. ANALYSIS TECHNIQUES

Extensive signal analysis was employed to extract ensemble-averaged characteristics and radial profiles of the density fluctuations. In addition to the usual correlation techniques, outlined in Sec. III A, we are able to compare the density fluctuations with individual toroidal harmonics of the magnetic fluctuations measured with a 32-position coil array and extract a toroidal mode number spectrum of the coherent density fluctuations. Once isolated, this coherent part, which is related to the global magnetic fluctuations, is used to extract radial profiles of the density fluctuations from the chordal measurements (Sec. III B).

A. Fluctuation and correlation analysis

To obtain meaningful statistics, correlations between fluctuating quantities are collected from large data ensembles. For this technique to be effective, it is important that the parameters in each data sample be similar. Periodic relaxation events, or sawteeth, are a robust feature of MST plasmas (Fig. 3). During the flattop phase of the discharge, when the plasma is nearest to steady state, the sawtooth cycle is very regular. The sawtooth crash time is a natural refer-

ence point about which to construct similar realizations. During PPCD discharges when the sawteeth are suppressed, realizations are chosen based on the PPCD firing time.

The correlation procedure for standard discharges amounts to segmenting the data into windows centered around the sawtooth crash time. Realizations (i.e., data segments) are chosen which begin 2 ms prior to a sawtooth crash and end at the crash. If required, the signals are frequency filtered, and the correlated products are ensemble averaged. This process yields a coherence amplitude and phase between the two fluctuating quantities and can be conducted in either the time or frequency domain. Correlations for PPCD plasmas are conducted in an identical manner with the exception that the time window is 3 ms wide, beginning 4 ms after PPCD starts.

Errors associated with this correlation technique are accurately described by Poisson statistics. The noise baseline for the coherence amplitude between two signals is inversely proportional to the square root of the number of realizations (i.e., $N_b \sim 1/\sqrt{n_{\text{events}}}$). The baseline has significance in determining the reliability of the phase measurement. The relative phase has meaning only if the amplitude of coherence is above the noise. Most of the ensembles presented in this study were obtained from over 400 events, yielding a noise baseline of about 0.05.

In addition to determining general coherent similarities between independent measurements, this correlation technique can be used to isolate fluctuation components of a specific helicity when a correlation with global magnetic modes is present. Since the magnetic coil arrays are used to decompose the magnetic fluctuations, as measured at the plasma edge, into their principal Fourier harmonics, correlation between any harmonic and a fluctuating quantity yields the coherent component with a given helicity.

B. Extracting density fluctuation profiles

Once the coherent part of the density fluctuation with a given m and n has been extracted, the local fluctuation profiles can be determined. The inversion method is similar to that used to obtain equilibrium density profiles with the exception that the helical nature of the perturbation must be considered. For fluctuations known to be poloidally symmetric (i.e., $m=0$), up/down symmetry is maintained and the inversion proceeds as it would for the equilibrium case. However the core-resonant tearing modes are $m=1$, and with symmetry violated the inversion process must be modified. This is accomplished by assuming the density perturbation takes the form of

$$n(r)=n_0(r)+\tilde{n}(r)\cos(\omega t+m\theta+n\phi+\delta(r)), \tag{2}$$

where ϕ and θ are toroidal and poloidal angles, and $\tilde{n}(r)$ and $\delta(r)$ are the radial functions of the amplitude and phase of the density fluctuation.

A chord integrated measurement of this perturbation can be written as

$$I(x)=I_0(x)+\tilde{I}(x), \tag{3}$$

where

$$\tilde{I}(x)=\int_{-L/2}^{+L/2}\tilde{n}(r)\cos(\omega t+m\theta+n\phi+\delta(r))\,dz. \tag{4}$$

Here, x represents the impact parameter of the chord, L is the chord's path length through the plasma, and z is the vertical coordinate. With a little algebra and a change in integration variable, Eq. (4) can be expressed as

$$\tilde{I}(x)=\tilde{I}_{\text{amp}}(x)\cos(\omega t+n\phi+\Delta(x)), \tag{5}$$

where we have introduced a chord-integrated amplitude,

$$\tilde{I}_{\text{amp}}(x)=2x\left[\left(\int_x^a\frac{\tilde{n}(r)\sin(\delta(r))}{\sqrt{r^2-x^2}}dr\right)^2+\left(\int_x^a\frac{\tilde{n}(r)\cos(\delta(r))}{\sqrt{r^2-x^2}}dr\right)^2\right]^{1/2} \tag{6}$$

and phase

$$\Delta(x)=\tan^{-1}\left[\frac{\int_x^a(\tilde{n}(r)\sin(\delta(r))/\sqrt{r^2-x^2})\,dr}{\int_x^a(\tilde{n}(r)\cos(\delta(r))/\sqrt{r^2-x^2})\,dr}\right]. \tag{7}$$

To extract the local density $[\tilde{n}(r)]$and phase $[\delta(r)]$ profiles, we distill Eqs. (6) and (7) into a more usable form. This is accomplished by relating the products of $\tilde{I}_{\text{amp}}(x)$ and the sine and cosine of the phase arriving at

$$\tilde{I}_{\text{amp}}(x)\sin(\Delta(x))=\int_x^a\frac{\tilde{n}(r)\sin(\delta(r))}{\sqrt{r^2-x^2}}dr \tag{8}$$

and

$$\tilde{I}_{\text{amp}}(x)\cos(\Delta(x))=\int_x^a\frac{\tilde{n}(r)\cos(\delta(r))}{\sqrt{r^2-x^2}}dr. \tag{9}$$

At this point, Eqs. (8) and (9) can be inverted in a manner similar to that outlined by Barr[27] to yield

$$\tilde{n}(r)\sin(\delta(r))=-\frac{r}{\pi}\int_r^a\frac{d}{dx}\left(\frac{\tilde{I}_{\text{amp}}(x)\sin(\Delta(x))}{2x}\right)\frac{dx}{\sqrt{x^2-r^2}} \tag{10}$$

and

$$\tilde{n}(r)\cos(\delta(r))=-\frac{r}{\pi}\int_r^a\frac{d}{dx}\left(\frac{\tilde{I}_{\text{amp}}(x)\cos(\Delta(x))}{2x}\right)\frac{dx}{\sqrt{x^2-r^2}}. \tag{11}$$

By correlating the fluctuating part of the integrated electron density with a specific Fourier component of the magnetic fluctuations ($\langle\tilde{I}\tilde{b}_{m,n}\rangle$), the chord integrated density fluctuation amplitude ($\tilde{I}_{\text{amp}}$) and phase (Δ) can be isolated. Having obtained the products $\tilde{I}_{\text{amp}}\sin(\Delta)$ and $\tilde{I}_{\text{amp}}\cos(\Delta)$ for each chord, an Abel inversion is conducted, and the radial functions $\tilde{n}(r)$ and $\delta(r)$ are extracted.

IV. DENSITY FLUCTUATION CHARACTERISTICS

During standard discharges, the chord-averaged density fluctuation amplitudes range from $\sim 3\%$ in the core to about 30% at the edge (Fig. 4). The frequency spectra for three

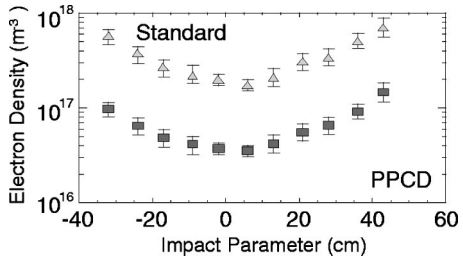

FIG. 4. Total chord-averaged electron density fluctuation amplitude from 1 to 100 kHz in both standard and high-confinement PPCD discharges. Averages obtained from 405 standard and 243 PPCD discharges.

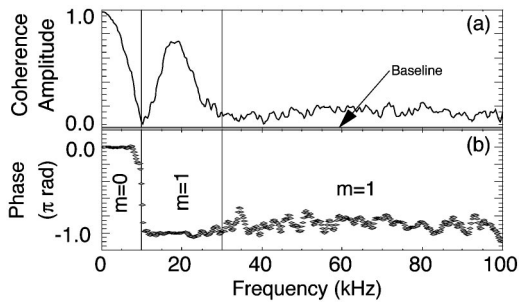

FIG. 6. Coherence amplitude (a) and phase (b) between $r/a=-0.62$ inboard and $r/a=0.83$ outboard FIR chords. Both chords are at the same toroidal angle. Ensemble consisted of 477 events with noise baseline of ~ 0.045.

different impact parameters ($r/a=0.11$, 0.54, and 0.83) are shown in Fig. 5. Clearly, the measurements at different radii are sensing different fluctuations. The measured fluctuations fall naturally into three groups: low (<10 kHz), medium (10–30 kHz), and high (>30 kHz) frequency.

Low frequency fluctuations are present at all radii. Correlations between different FIR chords (Fig. 6) demonstrate that these fluctuations are highly coherent and in phase across the entire plasma column (i.e., $m=$ even). Recalling that the interferometer is composed of 11 chords separated into two toroidally spaced (5°) vertical viewing arrays, two-point techniques can be applied to arrive at the toroidal mode-number spectrum. Figure 7 shows the average toroidal mode number versus frequency for an impact parameter of $r/a=0.58$. We see that for frequencies below 10 kHz, the fluctuations are dominated by low toroidal mode numbers. Figure 8(a) shows the toroidal mode-number spectrum, at 3 kHz, for the same chord location. The spectrum is peaked strongly at $n=0$, which corresponds to changes in the equilibrium. However some power is clearly present at $n=1-3$. These measurements indicate that fluctuations in the low frequency range arise from a mixture of slow changes in the mean density and long wavelength, poloidally symmetric, $m=0$ modes which are resonant near $r/a\sim 0.85$ where the toroidal magnetic field reverses.

Fluctuations in the medium frequency range (10–30 kHz) are of a different nature. Figure 5 shows that a peak appears at these frequencies in all but the central chords. The correlation of inboard and outboard chords, shown in Fig. 6, reveals that these fluctuations are also highly coherent across the entire plasma column but are π rad out of phase (i.e., $m=$ odd). Determination of the phase between all FIR chords show definitively that these fluctuations exhibit an $m=1$ nature. From Figs. 7 and 8(b), one can see that the toroidal mode number spectrum of these fluctuations peaks around $n=6$ and is broader than the spectrum at low frequency. The frequency and wave-number characteristics of these fluctuations correspond very well with the core-resonant modes which dominate RFP behavior. In Sec. V, we demonstrate that the density fluctuations in this frequency range are indeed well correlated with global core-resonant magnetic fluctuations. The lack of appreciable signal in central channels is due to the insensitivity of these chords to $m=$ odd perturbations.

Finally, we examine the character of fluctuations at frequencies above 30 kHz. These exist in all chords to some extent but are present at large amplitude only for those in the edge. The coherence between inboard and outboard chords (Fig. 6) is lower than that of other frequency ranges, indicating these fluctuations are more localized with shorter correlation lengths. Examination of the phase shows that the fraction which is coherent has an $m=1$ character. The mean toroidal mode number is large ($n\sim 35$) and the mode spectrum is very broad. These features are consistent with short wavelength electrostatic and magnetic fluctuations, particularly the $m=1$, high n fluctuations resonant in the edge on either side of the toroidal field reversal surface ($r/a\sim 0.85$).

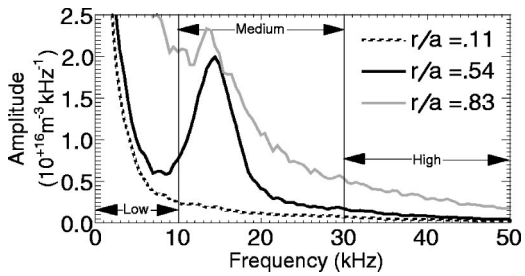

FIG. 5. Chord-averaged density fluctuation ($\tilde{n}$) amplitude spectra for impact parameters of $r/a=$ 0.11, 0.54, and 0.83. Amplitudes obtained from 477 realizations yielding a noise baseline of $\sim 0.1\times 10^{+16}$ m^{-3} kHz^{-1}.

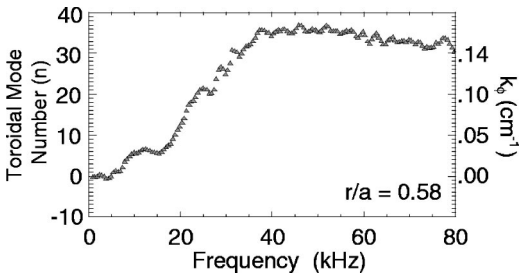

FIG. 7. The average toroidal mode number (n) and wave number (k_ϕ) for impact parameter $r/a=0.58$. Here, the average mode number is defined as the average of the measured n spectrum at a given frequency.

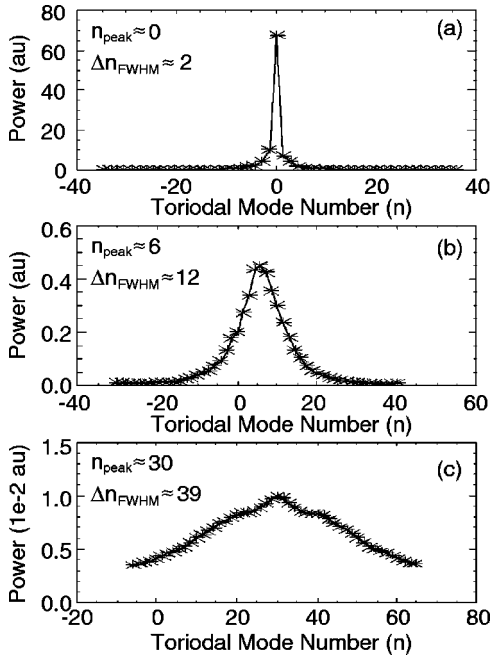

FIG. 8. The toroidal mode number (n) spectrum for (a) 3 kHz, (b) 18 kHz, and (c) 35 kHz at an impact parameter of $r/a=0.58$.

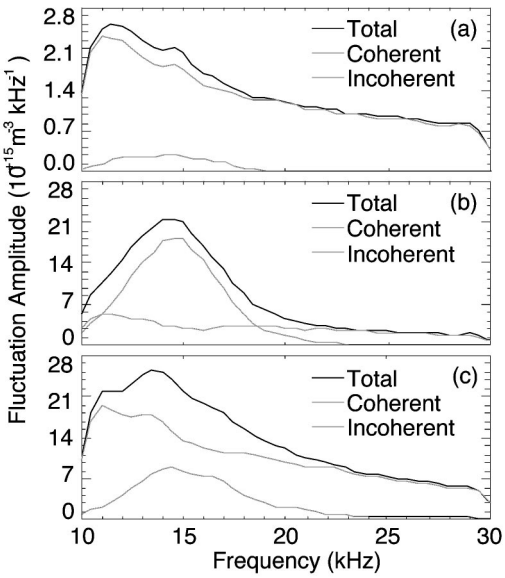

FIG. 9. The total, coherent, and incoherent density fluctuation power for impact parameters of $r/a=$ (a) 0.11, (b) 0.54, and (c) 0.83. Data from 1055 realizations with a noise baseline of $\sim 7.0\times 10^{+14}$ m^{-3} kHz^{-1}.

V. CORRELATION BETWEEN DENSITY AND MAGNETIC FLUCTUATIONS

We now describe the relationship between the observed density and magnetic fluctuations. In general, we find little correlation in the low and high frequency ranges. For frequencies of 10–30 kHz, however, density and magnetic field fluctuations are strongly correlated.

To determine the spatial harmonic content of the density fluctuations which arise from the global magnetic tearing fluctuations, we correlate the chord-integrated FIR measurements with the decomposed Fourier harmonics of the magnetic fluctuations obtained from the 32-position toroidal array of coils. The density fluctuation power that is coherent with the $m=1$, $n=5-15$ core-resonant tearing modes is displayed in Fig. 9, along with the total and incoherent fluctuation power for impact parameters of $r/a=0.11$, 0.54, and 0.83. We see that the center-most chord is poorly coherent with the magnetic fluctuations due to the insensitivity of central chords to $m=$odd perturbations [Fig. 9(a)]. At larger impact parameters, virtually all of the power between 10 and 20 kHz is coherent with $n=5-15$ modes [Fig. 9(b)]. In the plasma edge, the density fluctuations are less coherent with the core-resonant tearing modes as the relative contribution from smaller scale magnetic and electrostatic fluctuations increases [Fig. 9(c)].

Figure 10 contains the radial profile of the total, coherent, and incoherent density fluctuation power between 10 and 30 kHz. Again, we see in the core that virtually all the observed density fluctuations are incoherent with the $m=1$,$n=5-15$ tearing modes. However, as the impact parameter increases, the coherent fraction rises to a peak value of $\sim 90\%$ at r/a of ~ 0.6, only to fall at the extreme edge where the contribution from small-scale, high n fluctuations becomes more prominent.

The correlated product of the density and magnetic fluctuations can be used to extract the radial fluctuation profiles $[\tilde{n}(r)]$ as discussed briefly in Sec. III B. In standard discharges, the radial fluctuation profiles for the $m=1$, $n=6-9$ helicities are broad, with amplitudes $\sim 1\%$ [Figs. 11(a)–11(d)]. The density fluctuation profiles are hollow for all n. As will be shown in Sec. VI, a large part of the observed density fluctuations arise from advection of the mean density gradient by perturbed magnetic field lines moving past the interferometer. Hence, the amplitude is largest when either the density gradient or the radial magnetic field fluctuation is large. In MST the density gradient is largest in the edge, and therefore the density fluctuation profiles tend to be edge peaked. An interesting feature is that as n increases, the profiles become more hollow. This is consistent with the profile of radial magnetic field fluctuation moving out in radius for higher n. Such is expected from MHD computation and the simple fact that modes with higher n are resonant at larger radii.

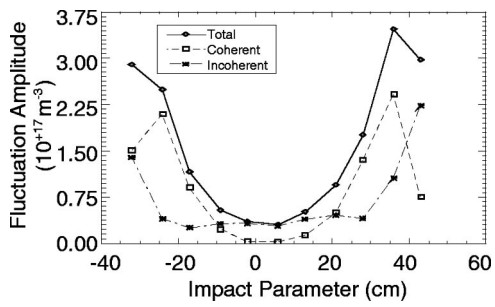

FIG. 10. The total amplitude of medium range (10–30 kHz) density fluctuations vs impact parameter. The coherent, and incoherent components are determined by correlation of FIR density measurements with the $n=5-15$ core-resonant magnetic modes.

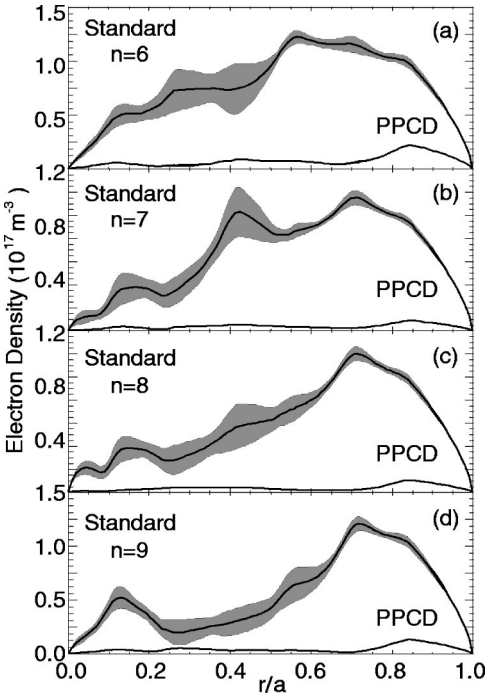

FIG. 11. Radial electron density fluctuation profiles $[\tilde{n}(r)]$ for the $m=1$ (a) $n=6$, (b) $n=7$, (c) $n=8$, and (d) $n=9$ toroidal components. Gray bands indicate profile variations from 500 Monte Carlo inversions.

VI. CORRELATION BETWEEN DENSITY AND RADIAL FLOW FLUCTUATIONS

We have established previously that the density fluctuations in the medium frequency range are associated with core-resonant tearing modes. Because of the global nature of these modes, it is possible to combine measurements made at different poloidal and toroidal positions to investigate the origin of the density fluctuations and their role in electron transport. In this section we report measurements of the plasma flow, which, when combined with measurements of density and magnetic field, give insight into the origin of the observed density fluctuations. We find that in the edge, the fluctuations are consistent with advection of the mean density gradient and no electron transport. In the core, the density fluctuations appear to be of a different origin and the relative phase between $\tilde{n}$ and $\tilde{v}_r$ allude that they may be inducing particle transport.

A. Relationship between density and radial velocity fluctuations

As discussed earlier, we employ fast Doppler spectroscopy to measure the chord-averaged radial flow of impurity ions. Because emission profiles are broad and measurements are made on a central chord, only odd *m*, large-scale fluctuations contribute significantly to the measured radial velocity. This is acceptable for measurement of core-resonant modes. Core and edge information is obtained by collecting light from different impurities as described in Sec. II B. To interpret the results, we assume that the fluctuating radial electron and impurity ion flow velocities are equal, as occurs if the flow arises from a fluctuating $E\times B$ drift. This assumption follows from MHD modeling of the RFP and is consistent with probe measurements conducted at the extreme plasma edge.[28,29]

The edge radial velocity fluctuations, measured via He II emission, are coherent with the core-resonant tearing modes. Moreover, these radial flow fluctuations, $\tilde{v}_r$, are in phase with the fluctuations in radial magnetic field, $\tilde{b}_r$, demonstrating a consistency with ideal MHD which predicts $\tilde{v}_r \propto k_{\text{parallel}}\tilde{b}_r$.

Combining edge measurements of density, radial flow, and radial magnetic field, we find that $\tilde{n}$ is $\pi/2$ rad out of phase with both $\tilde{v}_r$ and $\tilde{b}_r$. In addition, the density fluctuations are large in the region where the equilibrium density gradient is maximum. These results strongly suggest that these coherent edge density fluctuations result from the advection of the equilibrium density gradient, i.e., $\tilde{n}\propto i\tilde{v}_r\nabla n_o \propto ik_{\text{parallel}}\tilde{b}_r\nabla n_o$.

Information on the core $\tilde{v}_r$ is obtained from C V emission which comes primarily from the region $0<r/a<0.8$. We find that $\tilde{v}_r$ averaged over this region is very small. Since measurements with He II, which sample $r/a>0.6$, have already established the existence of radial velocity fluctuations in the edge, the nearly null result implies a radial velocity fluctuation whose phase changes by π in the core. This phase shift is consistent with the idealized picture of a tearing mode in which $\tilde{v}_r$ changes sign across the mode's resonant surface. Complete measurements of the radial profile of core-resonant $m=1$ velocity fluctuations await diagnostics with improved radial resolution.

Existing observations of the density and velocity fluctuations in the core indicate that these density fluctuations are of a different nature than those in the edge. The density, radial flow, and radial magnetic field fluctuations are all in phase (or π out of phase). The core density fluctuations cannot arise from advection of the equilibrium gradient but are instead the result of either compression, coherent fluctuations in the particle source term, nonlinear coupling, or some combination of these. This is significant since advection of equilibrium gradients cannot induce particle transport whereas these other effects may.

B. Fluctuation-induced electron transport

The phase relation between density and radial velocity fluctuations also provides key information on the fluctuation-induced particle transport (Fig. 12). The mean radial particle flux can be broken into two terms:

$$\Gamma_r=\langle nv_r\rangle=\langle n\rangle\langle v_r\rangle+\langle\tilde{n}\tilde{v}_r\rangle. \tag{12}$$

The first term is the flux due to transport of the mean density by mean radial flows and the second is the flux due to correlated density and flow fluctuations. Fluctuations can contribute to both terms although they appear explicitly only in the second. Since we measure both $\tilde{n}$ and $\tilde{v}_r$ for core-resonant modes, we can compute the contribution of density fluctuations to particle transport.

The second term in Eq. (12) can be represented as

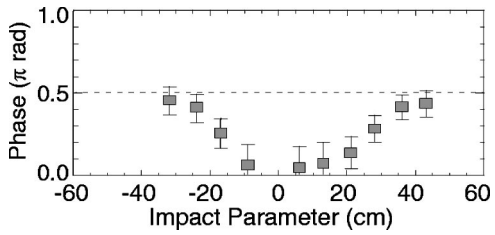

FIG. 12. Radial profile of the phase, averaged over 477 events, between the chord-averaged density fluctuations ($\tilde{\bar{n}}$) and edge radial velocity fluctuations ($\tilde{v}_{\mathrm{redge}}$).

$$\langle \tilde{n}\tilde{v}_r \rangle = \gamma |\tilde{n}||\tilde{v}_r| \cos(\delta_{nv}), \tag{13}$$

where γ is the coherence amplitude and δ_{nv} is the phase between $\tilde{n}$ and $\tilde{v}_r$. Since $\delta_{nv} \sim \pi/2$ in the outer region of the plasma ($r/a > 0.6$), the particle flux due to core-resonant density fluctuations is measured to be small. Therefore, although the core-resonant modes are relatively large in the edge, they do not cause particle transport. This is consistent with the idea that magnetic modes do not produce transport far from their resonant surfaces.

In the plasma core, where the modes are resonant, the density fluctuations exhibit a $\pi/2$ phase shift relative to the edge. With $\delta_{nv} \sim 0$, $\tilde{n}$ and $\tilde{v}_r$ couple to drive particle transport. Although the magnitude of $\tilde{v}_r$ in the core is unknown, estimates suggest that $\langle \tilde{n}\tilde{v}_r \rangle$ could be enough to account for all particle transport inside $r/a \sim 0.40$.

VII. REDUCTION OF DENSITY FLUCTUATIONS AND ELECTRON FLUX WITH AUXILIARY CURRENT DRIVE

The application of auxiliary current drive (PPCD) in MST has been shown to reduce magnetic fluctuations and improve global confinement substantially.[30] As shown in Fig. 4, density fluctuations are also reduced dramatically throughout the plasma. The density fluctuations associated with the core-resonant tearing modes drop by more than an order of magnitude and become more edge peaked [Figs. 11(a)–11(d)]. Local amplitudes range from ~0.05% in the core to about 0.1% near the edge. A remarkable feature that appears during PPCD discharges is that the radial phase shift in $\tilde{n}$ vanishes [Fig. 13(b)]. This suggests that $\tilde{n}$ and $\tilde{v}_r$ remain out of phase much deeper into the core. The change in phase, coupled with the order of magnitude reduction of $\tilde{n}$, indicates that the fluctuation-induced electron transport due to core-resonant density fluctuations is greatly reduced in the core.

The dramatic decrease in the fluctuation amplitudes during PPCD is accompanied by similar reductions in the total radial electron flux (Γ_r). Figures 14(a)–14(c) present the electron density, source and radial flux profiles as measured in both standard and PPCD-induced higher confinement plasmas. In standard plasmas, the electron density profile is flat over much of the plasma cross section with a very steep gradient at the edge. The electron source profile, which results primarily from the ionization of neutral hydrogen (deuterium), is edge peaked but with substantial sourcing occurring in the plasma core [Fig. 14(b)]. This results in radial electron flux, shown in Fig. 14(c), that ranges from $\sim 2.0 \times 10^{+20}$ $\mathrm{m^{-2}\,s^{-1}}$ in the core rising to $\sim 3.0 \times 10^{+21}$ $\mathrm{m^{-2}\,s^{-1}}$ at the plasma boundary. During PPCD discharges, when the density fluctuation amplitudes are reduced, it is quite common to see the electron density increase by as much as 50%. In an attempt to maintain similar profile amplitudes for both cases, the initial fueling was reduced such that at peak confinement, the total particle content would be comparable. As a result, the electron density profiles measured during auxiliary current drive have similar magnitudes, but unlike the standard case, show a hollowness developing in the core [Fig. 14(a)]. This gradient formation in the core is a clear indicator of confinement improvement. Moreover in the core, the electron source drops dramatically [Fig. 14(b)] as the contribution from neutral hydrogen (deuterium) ionization falls to such low levels that virtually all core sourcing results from impurities. The overall radial par-

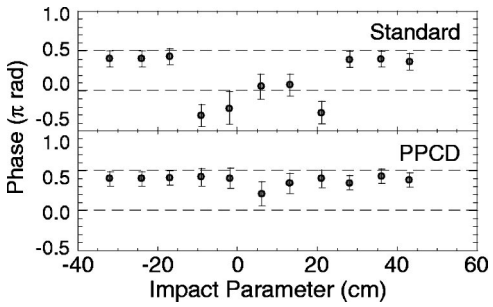

FIG. 13. Radial profile of the phase between the chord-averaged density fluctuations ($\tilde{\bar{n}}$) and edge radial magnetic field fluctuations for (a) standard and (b) PPCD discharges. During PPCD the density fluctuations in the core change phase relative to those in the edge. Ensembles conducted over 405 standard and 243 PPCD events. The error bars are smaller in the PPCD case because the core fluctuations are actually more coherent, thus the phase is more accurately resolved.

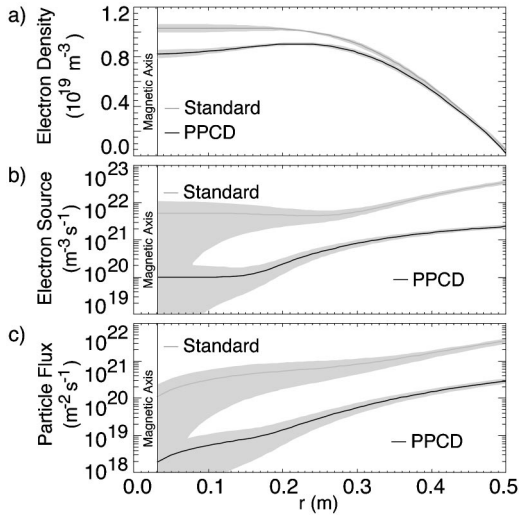

FIG. 14. Radial profiles of (a) electron density, (b) electron source (impurities included), and (c) radial electron flux for standard and PPCD discharges. The gray bands indicate profile variations from 500 Monte Carlo inversions.

ticle flux also drops [Fig. 14(c)]. In the core, the reduction is almost two orders of magnitude, yielding an average flux $\sim 2.0\times 10^{+18}$ $\mathrm{m}^{-2}\,\mathrm{s}^{-1}$ for $r/a<0.3$.

VIII. CONCLUSION

In summary, simultaneous measurements of the fluctuating density, radial velocity, and magnetic field elucidate the cause of the density fluctuations and electron transport in the RFP. We find that density fluctuations fall naturally into three categories corresponding to low (<10 kHz), medium (10–30 kHz), and high (>30 kHz) frequencies. The fluctuations in the 10–30 kHz range are dominantly core resonant and are highly coherent with both magnetic and velocity fluctuations. Moreover, these fluctuations are advective in the edge but not in the core. Direct measurement of $\langle \tilde{n}\tilde{v}_r \rangle$ in the outer region of the plasma reveals that density fluctuations associated with core-resonant magnetic fluctuations do not cause measurable electron transport at the edge. In the core the radial velocity measurements are inconclusive, but suggest that density fluctuations do contribute to significant transport in standard discharges. During PPCD discharges, in which auxiliary current drive is applied to improve global confinement, the radial electron flux decreases dramatically throughout the plasma. Furthermore, density fluctuations decrease, and the phase of the fluctuations changes in the core. This indicates a severe reduction in the fluctuation-induced electron transport in the core.

An important caveat to these measurements is that the chord-averaged nature of the density and velocity fluctuation measurements limits the spatial resolution. Hence these measurement techniques are only appropriate for large-scale fluctuations. Therefore, more localized fluctuations which may drive transport are not addressed here. Additional diagnostics, such as charge-exchange recombination spectroscopy and a heavy ion beam probe, are being applied to provide better localized measurements of both density and velocity fluctuations.

IX. ACKNOWLEDGEMENTS

The authors are especially grateful for the contributions of J. T. Chapman, P. W. Fontana, D. Holly, J. S. Sarff, and the MST group.

This work was supported by the U.S. Department of Energy.

[1] H. A. B. Bodin and A. A. Newton, Nucl. Fusion **19**, 1255 (1980).
[2] M. R. Stoneking, S. A. Hokin, S. C. Prager, G. Fiksel, H. Ji, and D. J. Den Hartog, Phys. Rev. Lett. **73**, 549 (1994).
[3] G. Fiksel, S. C. Prager, W. Shen, and M. Stoneking, Phys. Rev. Lett. **72**, 1028 (1994).
[4] T. D. Rempel, C. W. Spragins, S. C. Prager, S. Assadi, D. J. Den Hartog, and S. Hokin, Phys. Rev. Lett. **67**, 1438 (1991).
[5] H. Ji, H. Toyama, K. Miyamoto, S. Shinohara, and A. Fujisawa, Phys. Rev. Lett. **67**, 62 (1991).
[6] J. S. Sarff, S. A. Hokin, H. Ji, S. C. Prager, and C. R. Sovinec, Phys. Rev. Lett. **72**, 3670 (1994).
[7] J. S. Sarff, N. E. Lanier, S. C. Prager, and M. R. Stoneking, Phys. Rev. Lett. **78**, 62 (1997).
[8] R. Bartiromo, V. Antoni, T. Bolzonella, A. Buffa, L. Marrelli, P. Martin, E. Martines, S. Martini, and R. Pasqualotto, Phys. Plasmas **6**, 1830 (1999).
[9] A. R. Jacobson, Plasma Phys. **23**, 927 (1981).
[10] A. R. Jacobson, Plasma Phys. **24**, 1111 (1982).
[11] S. Masamune, Phys. Fluids **31**, 1231 (1988).
[12] J. C. Ingraham, R. F. Ellis, J. N. Downing, C. P. Munson, P. G. Weber, and G. A. Wurden, Phys. Fluids B **2**, 143 (1990).
[13] P. G. Weber, K. F. Schoenberg, J. C. Ingraham *et al.*, Plasma Phys. Controlled Fusion **2**, 509 (1990).
[14] G. A. Wurden, P. G. Weber, K. F. Schoenberg *et al.*, ''Ion heating studies in the ZT-40M reversed field pinch,'' *15th European Conference on Controlled Fusion and Plasma Heating, Dubrovnik, 16–20, May 1988* (European Physical Society, Petit-Lancy, 1989), Vol. 12B, Part II, p. 533.
[15] D. A. Baker, C. J. Buchenauer, L. C. Burkhardt *et al.*, ''Experimental and theoretical studies of the ZT-40M reversed-field pinch,'' *Proceedings of the Tenth International Conference Plasma Physics and Controlled Nuclear Fusion Research, London, 12–19, September 1984* (International Atomic Energy Agency, Vienna, 1985), Vol. 2, p. 439.
[16] R. N. Dexter, D. W. Kerst, T. W. Lovell, S. C. Prager, and J. C. Sprott, Fusion Technol. **19**, 131 (1991).
[17] N. E. Lanier, D. Craig, J. K. Anderson, T. M. Biewer, B. E. Chapman, D. J. Den Hartog, D. B. Forest, S. C. Prager, D. L. Brower, and Y. Jiang, Rev. Sci. Instrum. **72**, 1039 (2001).
[18] Y. Jiang, N. E. Lanier, and D. L. Brower, Rev. Sci. Instrum. **70**, 703 (1999).
[19] S. R. Burns, W. A. Peebles, D. Holly, and T. Lovell, Rev. Sci. Instrum. **63**, 4993 (1992).
[20] D. W. Choi, E. J. Powers, R. D. Bengtson, G. Joyce, D. L. Brower, W. A. Peebles, and N. C. Luhmann, Jr., Rev. Sci. Instrum. **57**, 1989 (1986).
[21] Y. Jiang, D. L. Brower, L. Zeng, and J. Howard, Rev. Sci. Instrum. **68**, 902 (1997).
[22] D. J. Den Hartog and R. J. Fonck, Rev. Sci. Instrum. **68**, 3238 (1994).
[23] J. T. Chapman and D. J. Den Hartog, Rev. Sci. Instrum. **68**, 285 (1996).
[24] L. C. Johnson and E. Hinnov, J. Quant. Spectrosc. Radiat. Transf. **13**, 333 (1973).
[25] N. E. Lanier, S. P. Gerhardt, and D. J. Den Hartog, Rev. Sci. Instrum. **72**, 1188 (2001).
[26] R. A. Hulse, Nucl. Technol./Fusion **3**, 259 (1983).
[27] W. M. Barr, J. Opt. Soc. Am. **52**, 885 (1962).
[28] H. Ji, A. F. Almagri, S. C. Prager, and J. S. Sarff, Phys. Rev. Lett. **73**, 668 (1994).
[29] P. W. Fontana and G. Fiksel, Bull. Am. Phys. Soc. **44**, 10 (1999).
[30] N. E. Lanier, D. Craig, J. K. Anderson, T. M. Biewer, B. E. Chapman, D. J. Den Hartog, D. B. Forest, S. C. Prager, D. L. Brower, and Y. Jiang, Phys. Rev. Lett. **85**, 2120 (2000).